THE JOURNAL OF PHYSICAL CHEMISTRY A

 VOLUME 108, NUMBER 27, JULY 8, 2004

ARTICLES

Ultrafast Excited State Dynamics of Tri- and Hexaporphyrin Arrays

Ana Morandeira,[†,#] Eric Vauthey,[*,†] Anne Schuwey,[‡] and Albert Gossauer[‡]

Department of Physical Chemistry of the University of Geneva, 30 quai Ernest Ansermet, CH-1211 Genève 4, Switzerland, and Department of Chemistry of the University of Fribourg, Pérolles, CH-1700 Fribourg, Switzerland

Received: February 15, 2004; In Final Form: April 6, 2004

An investigation of the ultrafast excited state dynamics of triporphyrin and hexaporphyrin arrays consisting of covalently linked Zn tetraphenylporphine (ZnTPP) and free base tetraphenylporphine (FbTPP) units is reported. The interchromophoric distance in the hexamers is of the order of 13 Å, while it varies from 26 to 70 Å in the trimers. These arrays exhibit several features that differ substantially from those of the monomeric units: a broadening of the Soret band, a shortening of the S_2 lifetime of the ZnTPP chromophores, and additional ultrafast decay components of the S_1 fluorescence. In the hexaporphyrin arrays, most of these features are attributed to the presence of excitonic states that result from the strong coupling between the $B_{x,y}$ transition dipoles. The time constants for S_1 energy transfer between ZnTPP chromophores as well as between ZnTPP and FbTPP moieties, deduced from anisotropic and isotropic time-resolved fluorescence measurements, were found to be of the order of a few tens of picoseconds. Moreover, back energy transfer from the FbTPP to ZnTPP units is also observed. At high to moderate excitation intensity, S_1-S_1 annihilation becomes an important decay mechanism of the excited state population of the hexaporphyrins. In the triporphyrins, the differences relative to the monomer are ascribed to the interaction with the phenylacetylene linkers, which lifts the degeneracy of the S_2 states. S_2 and S_1 energy transfer were found to take place in the triporphyrin with the shortest linker only. In the other triporphyrins, an efficient energy transfer from the linker to the porphyrin units was observed.

Introduction

Over the past few years, intensive experimental and theoretical efforts have been invested to understand the energy transport mechanisms in photosynthetic light-harvesting complexes.[1−8] Although all the fine details of the excitation energy transfer (EET) are still not totally understood, it is well-known that the overall EET efficiency of these antenna complexes is very high. This large efficiency has stimulated the elaboration of mimics of these natural systems. One approach is the synthesis of large arrays of covalently linked chromophores with a specific design in order to fulfill several important criteria such a large collection efficiency and a fast and efficient energy migration to a well-defined energy trap. Like the natural antennae, most of these synthetic systems are based on porphyrin pigments.[9−27] These arrays are not only interesting as mimics of natural light-harvesting systems but may have potential application in molecular electronics and photonics.[28]

The major parameter for a light-harvesting system is the interaction between the chromophores. In natural antennae, the

* Corresponding author. E-mail: eric.vauthey@chiphy.unige.ch.
† University of Geneva.
‡ University of Fribourg.
# Present address: Department of Physical Chemistry of the University of Uppsala, 751 23 Uppsala, Sweden.

10.1021/jp049319m CCC: $27.50
Published on Web 06/11/2004

CHART 1: Nonoptimized Structure of the Porphyrin Arrays

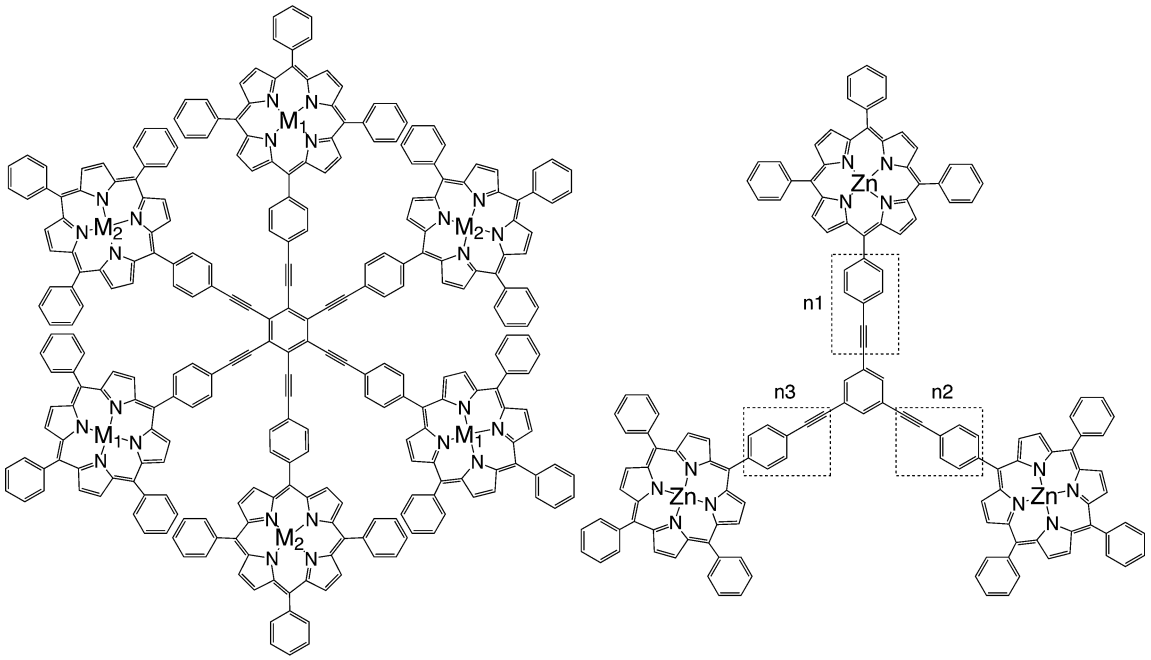

HZn_6: $M_1 = M_2 = Zn$
HFb_6: $M_1 = M_2 = 2H$
HZn_3Fb_3: $M_1 = Zn$, $M_2 = 2H$

TZn_3: n1 = n2 = n3 = 1
TZn_3L: n1 = n2 = n3 = 5
TZn_3D: n1 = 1, n2 = 3, n3 = 5

TABLE 1: Through-Space (TS) and Through-Bond (TB) Center to Center Distances between Adjacent Porphyrin Units

array	R_{TS} (nm)	R_{TB} (nm)
TZn_3	2.30	2.65
TZn_3L	6.97	8.05
TZn_3D (PA_5-PA_3)[a]	5.84	6.7
TZn_3D (PA_5-PA_1)	4.83	5.35
TZn_3D (PA_3-PA_1)	3.53	4.0
HZn_6	1.33	2.65
HZn_3Fb_3	1.33	2.65

[a] PA_n: linker with *n* PA units.

Coulombic interaction has been found to be the dominant EET mechanism.[2] In the weak interaction limit, the excitation is localized on a single chromophore and the EET can be discussed within the framework of the Förster theory.[29] In this case, the UV−vis absorption spectrum of the aggregate should be the composite of those of the individual chromophores. If the interaction is strong, the excitation is no longer localized on a single pigment. In this case, the presence of excitonic states with different energies leads to substantial changes in the UV−vis absorption spectrum compared to that of the individual pigments. Such strong coupling has been observed in porphyrin arrays with short interchromophoric distance.[24,25,30−34]

In covalently linked porphyrin arrays, the exchange interaction can also be operative, depending on the interchromophoric distance, on the nature of the linker, and on the position of the connection on the porphyrin ring.[35−40]

We present here an investigation of the excited state dynamics of the six porphyrin arrays depicted in Chart 1 using femtosecond fluorescence up-conversion upon Soret band (B-band) excitation, as well as steady-state fluorescence excitation anisotropy. The through-space (TS) and through-bond (TB) interchromophoric distances are listed in Table 1. The excited state dynamics of TZn_3 upon Q-band excitation (S_0-S_1) has already been studied.[40] It was found that S_1 EET between the ZnTPP units was quite efficient, with a time constant of $\tau_{EET} = 225$ ps. The TB distance in HZn_6 is the same as in TZn_3, but the TS distance is twice as small. Therefore, a much faster EET dynamics can be expected. Moreover, a dependence of the EET dynamics on the excitation, Q- or B-band, has to be considered. Indeed, the S_2 lifetime of ZnTPP is of the order of 2 ps and the $B_{x,y}$ transition dipoles are very large.[41] These two factors could a priori enable S_2 EET, especially in HZn_6, HZn_3Fb_3, and TZn_3. For a better understanding of HZn_3Fb_3, the excited state properties of the FbTPP hexamer, HFb_6, were investigated as well. Finally, in order to obtain a better insight into the role of the PA linkers on the excited state properties of the porphyrin units, triporphyrin arrays with very long linkers, TZn_3L, and with linkers of different length, TZn_3D, were also studied.

Experimental Section

Steady-State Measurements. UV−vis absorption spectra were recorded on a Cary 50 spectrometer, and fluorescence spectra were measured with a Cary Eclipse fluorometer. For the measurements of fluorescence excitation anisotropy (FEA) spectra, sheet polarizers were inserted in the path of the excitation beam and in front of the photodetector. The fluorescence anisotropy, *r*, was calculated as

$$r = \frac{I_{||} - GI_{\perp}}{I_{||} + 2GI_{\perp}} \quad (1)$$

where $I_{||}$ and $I_{\perp}$ are the fluorescence intensity components parallel and perpendicular to the polarization of the excitation beam, respectively, and *G* is a correction factor for the different sensitivity of the detector to horizontally and vertically polarized light. This factor was obtained from the ratio of $I_{||}/I_{\perp}$ measured with horizontally polarized excitation. These measurements were performed in viscous paraffin oil in order to prevent anisotropy decay by reorientational diffusion.

Time-Resolved Fluorescence. Measurements with low time resolution were performed by time-correlated single photon counting (TCSPC). The setup has been described in detail in ref 42. Excitation was performed at 395 nm with a pulsed laser diode (Picoquant model LDH-P-C-400B). The average power at 20 MHz was 0.5 mW, and the pulse duration around 65 ps. The full width at half-maximum (fwhm) of the instrument response function was less than 200 ps.

The fluorescence up-conversion setup has been described in ref 43. The 400 nm pump intensity on the sample was of the order of 10^{13} photons cm^{-2} $pulse^{-1}$. The polarization of the pump pulse could be varied with respect of that of the gate pulse with a Berek compensator. The fwhm of the instrument response function was 210 fs.

Samples. The synthesis of the hexamers, HZn_6, HFb_6, and HZn_3Fb_3, has been described in detail in ref 44 while that of TZn_3 and TZn_3L has been described in refs 19 and 40. TZn_3D has been synthesized analogously to compound **14** in ref 19. Toluene (Fluka, UV quality) and paraffin oil (Fluka, puriss., 100−230 mPa·s) were used without further purification. The concentration of the porphyrin arrays was adjusted to obtain an absorbance at the excitation wavelength of about 0.1 over 1 cm for TCSPC and of 0.1 over 0.4 mm for up-conversion measurements. This corresponds to concentrations of arrays sufficiently small ($\leq 10^{-5}$ M) to prevent photoinduced bimolecular processes. All solutions were bubbled with Ar for 15−20 min before use. No significant degradation of the samples was observed after the measurements.

Data Analysis. The fluorescence time profiles were analyzed by the iterative reconvolution of the instrument response function with trial functions (sum of exponentials) using a nonlinear least-squares fitting procedure (MATLAB, The MathWorks, Inc.).

Results

Absorption Spectra. The absorption spectra of all arrays exhibit Q- and B-bands such as those of the porphyrin monomers.[45] In the Q-band region (500−650 nm), the absorption spectra of ZnTPP arrays are very similar to that of the monomer, the main difference being a weak change of the relative intensity of the Q(1,0) and Q(0,0) bands. For HZn_6 and the triporphyrins, the absorption coefficient of these bands is respectively 6 and 3 times as large as that of ZnTPP. Figure 1 shows that larger differences exist in the B-band region. For the triporphyrins, this band is slightly broader and shifted to longer wavelength by about 5 nm. The B-band of HZn_6 is almost twice as broad as that of ZnTPP. For all these arrays, the B-band area divided by the number of chromophores is essentially the same.

The inset of Figure 1 shows that the absorption spectra of TZn_3L and TZn_3D exhibit additionally a broad band with a maximum around 350 nm. This band, which is not present in the spectra of the other arrays, is due to the linkers with 3 and 5 PA units, PA_3 and PA_5, the linker with a single PA unit, PA_1, absorbing below 300 nm.

The absorption spectrum of HFb_6 in the Q-band region is very similar to that of FbTPP and consists of four bands. Only small differences in the relative intensity of the $Q_y(0,0)$ and $Q_y(1,0)$ bands can be noticed. As for HZn_6, the B-band of HFb_6 is broader by a factor of about two than that of the monomer, the band area being six times larger than that of FbTPP.

The absorption spectrum of HZn_3Fb_3 cannot be reproduced by a linear combination of ZnTPP and FbTPP spectra, especially in the B-band region. However, it is the perfect 1:1 composite of the absorption spectra of HZn_6 and of HFb_6 as shown in Figure 1B.

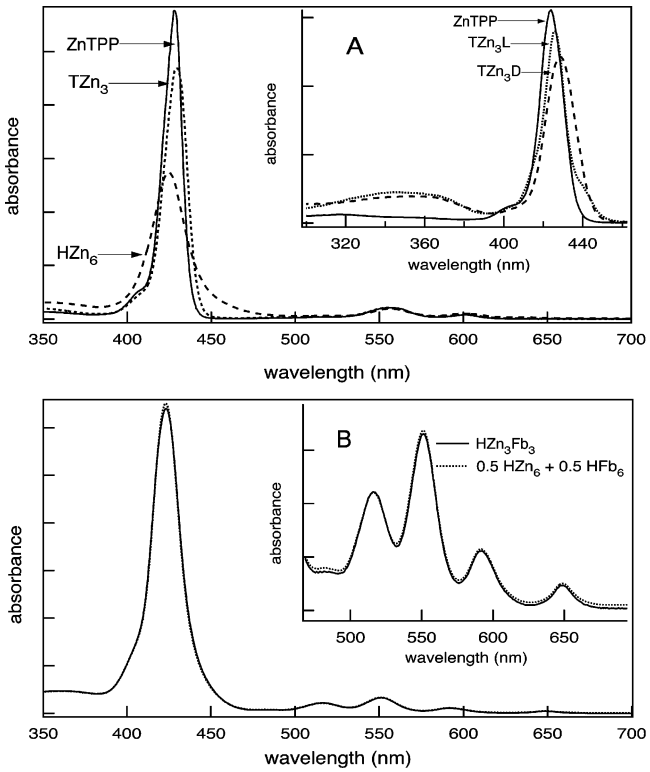

Figure 1. (A) Absorption spectra of HZn_6, TZn_3, and ZnTPP in toluene. Inset: Absorption spectra of TZn_3L, TZn_3D, and ZnTPP below 450 nm. (B) Absorption spectrum of HZn_3Fb_3 in toluene and composite spectrum of the absorption spectra of HZn_6 and of HFb_6.

Fluorescence Spectra. All ZnTPP arrays exhibit S_1 fluorescence in the 600−700 nm region. The fluorescence spectra of the triporphyrins are very similar to that of ZnTPP and consist of two bands around 600 and 650 nm that can be assigned to the Q(0,0) and Q(0,1) transitions, respectively. However, some differences in their relative intensity can be observed, as illustrated in Figure 2A. For ZnTPP, the Q(0,1) band is the most intense, while the opposite is observed with the triporphyrin arrays. However, the fluorescence yields of these arrays are essentially the same as that of ZnTPP.

Additionally to S_1 fluorescence, the triporphyrin arrays exhibit, like ZnTPP, an S_2 fluorescence band with a maximum between 425 and 435 nm (see Figure 2A). The S_2 emission maximum of the arrays is red shifted by a few nanometers compared to that of ZnTPP, and the fluorescence quantum yield is apparently smaller. However, it should be noted that the measurement of this emission is delicate because of its weakness and of the small Stokes shift. Therefore, the determination of the S_2 fluorescence yield and of the emission maximum is difficult.

The hexaporphyrins show S_1 fluorescence only. Compared to ZnTPP, the emission spectrum of HZn_6 is red shifted by 15 nm and the Q(0,1) band appears as a shoulder (see Figure 2A). Its fluorescence quantum yield was found to be essentially the same as that of ZnTPP. Taking the literature value of Φ_{fl}(ZnTPP) = 0.033[46] results in a fluorescence quantum yield of 0.030 for HZn_6.

HFb_6 and FbTPP fluorescence spectra are practically identical and consist of two bands at 655 and 715 nm that can be assigned to $Q_x(0,0)$ and $Q_x(0,1)$ transitions, respectively. This similarity is consistent with that observed with the Q_x-bands in the absorption spectra. The fluorescence quantum yield of HFb_6 was found to be slightly larger than that of the monomer. With

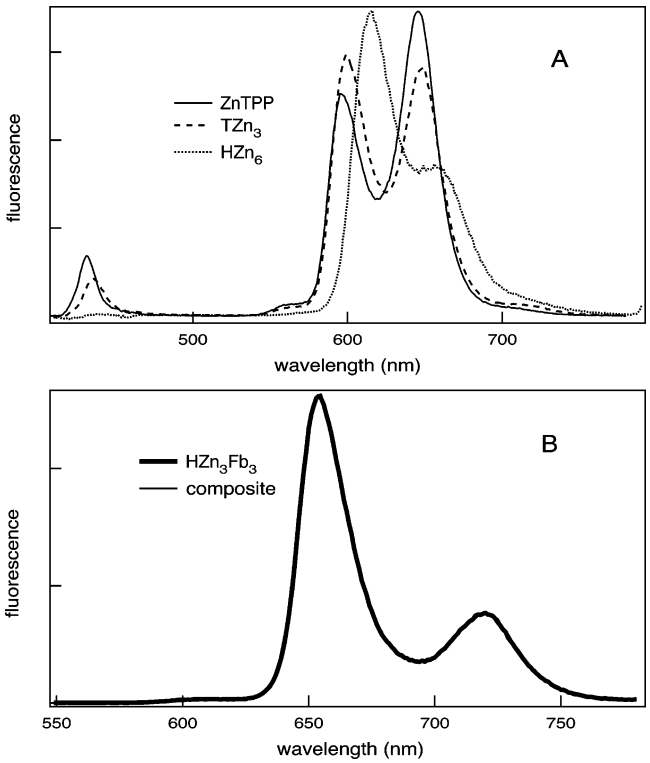

Figure 2. Fluorescence spectra of (A) HZn_6, TZn_3, and ZnTPP and (B) HZn_3Fb_3 in toluene and composite spectrum of the fluorescence spectra of HZn_6 and HFb_6.

use of the value of $\Phi_{fl}(FbTPP) = 0.11$,[47] a fluorescence quantum yield of 0.12 is obtained for HFb_6.

The fluorescence spectrum of the mixed array HZn_3Fb_3 is shown in Figure 2B. This spectrum is totally independent of the excitation wavelength. The band at 715 nm can be clearly ascribed to the $Q_x(0,1)$ transition of the FbTPP units, while the small pedestal around 610 nm arises from the ZnTPP units. This spectrum can be perfectly reproduced by a linear combination of the fluorescence spectra of HZn_6 and HFb_6. The areas of these spectra were normalized according to the radiative rate constant of ZnTPP ($k_{rad} = 1.8 \times 10^7\ s^{-1}$) and FbTPP ($k_{rad} = 9.2 \times 10^6\ s^{-1}$), respectively. With these values, the relative weights of the HZn_6 and HFb_6 spectra are 0.01 and 0.99, respectively.

The emission spectrum of all these arrays is independent of the excitation wavelength. For TZn_3L and TZn_3D, excitation in the broad absorption band located below 400 nm and due to the PA linkers results in the same fluorescence spectrum as direct excitation of the porphyrin chromophores.

Steady-State Anisotropic Measurements. In order to obtain more information on the origin of the spectral differences between ZnTPP and the ZnTPP arrays, fluorescence excitation anisotropy (FEA) spectra have been recorded. Figure 3 shows such a FEA spectrum measured with ZnTPP at the maximum of the Q(0,0) emission band. The anisotropy value in the B- and Q(1,0)-bands region is around 0.1. This value is consistent with the fact that the S_1 fluorescence is associated with two perpendicular and degenerate transition dipoles. For HZn_6 and TZn_3, the anisotropy is very small ($r = 0.02 \pm 0.02$), independent of the excitation wavelength. The situation is different for the other triporphyrin arrays as shown in Figure 3. For TZn_3L and TZn_3D, the fluorescence anisotropy upon Q(1,0) excitation amounts to 0.11 ± 0.02 and 0.125 ± 0.01, respectively. The situation is more complex in the B-band region, where the FEA spectrum is bipolar for both arrays. For TZn_3L,

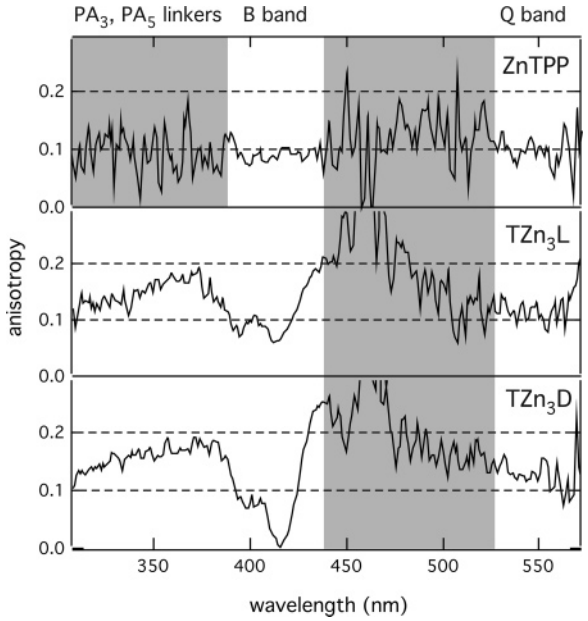

Figure 3. Fluorescence excitation anisotropy spectra of ZnTPP, TZn_3L, and TZn_3D in paraffin oil recorded at the maximum of the Q(0,0) emission band. The shaded areas represent the regions without absorption, where the anisotropy value should be discarded.

the anisotropy increases from 0.06 to about 0.2 upon varying the excitation from 413 to 433 nm, the anisotropy upon excitation at the maximum of the B-band being around 0.09. A similar but more pronounced effect is observed with TZn_3D, the anisotropy increasing from 0 to about 0.25 by going from 414 to 436 nm.

For these two triporphyrins, some anisotropy can also be observed upon excitation in the PA linker bands located below 400 nm. The anisotropy is not constant over the whole absorption band but increases from about 0.12 to 0.17 by going from around 310 to 370 nm.

Excitation Intensity Dependence of the Fluorescence Quantum Yield. It is well-known that exciton or S_1-S_1 annihilation can be a major deactivation pathway of excited states in chromophore aggregates.[48,49] Because of this, the excited state dynamics depends strongly on the excitation intensity, and therefore the investigation of the other deactivation pathways is problematic. The safest way to avoid this complication is to work at sufficiently low excitation intensity to ensure that the probability to have more that one excitation per aggregate is negligibly small. In the present case, S_1-S_1 annihilation could occur predominantly with the hexaporphyrins. In order to determine the excitation regime at which this process is negligible, an investigation of the dependence of the fluorescence quantum yield on the excitation intensity has been carried out. For these measurements, excitation was performed at 400 nm with the frequency-doubled output of an amplified Ti:Sapphire system, and the emitted fluorescence was detected by a CCD camera connected to a spectrograph. Figure 4 shows the fluorescence intensity of HZn_6 integrated over the whole spectrum, I_{fl}, divided by the excitation intensity, I_E, as a function of I_E. This figure shows that the fluorescence yield drops by a factor of about 3 by increasing the excitation intensity from 0.2 to 4 mJ/cm^2, indicating the occurrence of S_1-S_1 annihilation in HZn_6. The fluorescence yield of the ZnTPP in the same excitation regime shows only a weak saturation effect at the highest of I_E values. This rules out saturation as the origin of the intensity dependence of the fluorescence yield of HZn_6. A qualitatively similar intensity dependence was found with HFb_6

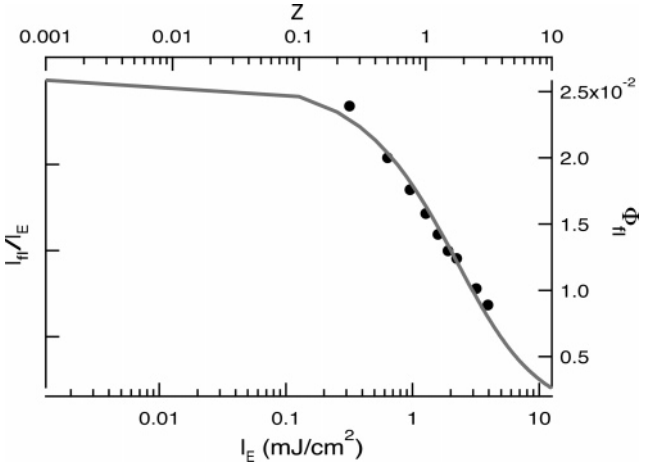

Figure 4. Integrated S_1 fluorescence intensity of HZn_6, I_{fl}, as a function of the excitation intensity, I_E (black circles), and best fit of eq 2 (solid line). The right and the top axes are the fluorescence quantum yield and the average number of excitation per array, respectively.

and HZn_3Fb_3. The solid line in this figure is the best fit of the following equation proposed by Paillotin and co-workers:[50]

$$\Phi_{fl}(Z) = \Phi_{fl}(0)\frac{(1 - e^{-Z})}{Z} \qquad (2)$$

where $\Phi_{fl}(0)$ is the fluorescence quantum yield in the low excitation intensity limit and Z is the average number of excitations per array. Equation 2 is a limiting case of a more general expression and is only valid to describe systems where the annihilation rate constant is much larger than the rate constant of unimolecular excited state decay. The fit of eq 2 to the experimental data allows the excitation intensity to be related to the average number of excitations per array (see Figure 4). Once Z is known, the population of arrays with n excitations ($0 \le n \le 6$) can be determined. For sufficiently small Z ($Z \le 1$), the probability, P_n, to have n excitations per array is given by a Poisson distribution, $P_n = Z^n e^{-Z}/n!$. For example, at the smallest excitation intensity used for this experiment, Z amounts to 0.25 and $P_1 = 0.195$, $P_2 = 0.024$, and $P_{n>2} \approx 0$. This means that when performing a measurement at this intensity, more than 10% of the excited arrays can experience S_1-S_1 annihilation. This contribution to the excited state dynamics might be strong enough to complicate the interpretation of the data.

In order to definitely avoid this problem, the excited state dynamics of the arrays was investigated by time-resolved fluorescence using sub-nJ pulses. For these measurements, the excitation intensity was less than 0.01 mJ/cm^2. According to the fit of eq 2 to the data shown in Figure 4, this corresponds to a Z value of less than 0.008 and the probabilities are thus: $P_1 = 7.9 \times 10^{-3}$, $P_2 = 3 \times 10^{-5}$, and $P_{n>2} \approx 0$. Moreover, eq 2 indicates that $\Phi_{fl}(0.008) = 0.996(\Phi_{fl}(0))$. Under these conditions, the contribution of S_1-S_1 annihilation to the fluorescence decay can be safely neglected.

Time-Resolved Isotropic Measurements. The fluorescence dynamics of the porphyrin arrays has been investigated in the nanosecond and subnanosecond time scale by TCSPC and in the picosecond and subpicosecond time scale by fluorescence up-conversion. No dependence of the fluorescence dynamics on the excitation intensity was observed in the low excitation intensity regime used. The data were analyzed by iterative reconvolution of a sum of exponential functions with the instrument response function. The lifetimes of the slow fluorescence decay components (>1 ns) were extracted from the TCSPC data. These lifetimes were used as fixed parameters when analyzing the fluorescence up-conversion data. The up-conversion measurements have been performed in several time windows, and the data were analyzed globally. Table 2 lists the best-fit parameters related to the S_2 fluorescence and to the rise of the S_1 fluorescence, while Table 3 shows those related to the decay of the S_1 fluorescence. For comparison, the fluorescence dynamics of ZnTPP and FbTPP monomers in toluene is also reported. The fluorescence dynamics of these monomers is consistent with that found in previous investigations in aromatic solvents.[43,51,52]

TABLE 2: S_2 Fluorescence Lifetimes at 440 nm and S_1 Fluorescence Rise Times Measured with ZnTPP and the Arrays[a]

compound	τ_{S2} (ps)	$\tau_{r,S1}$ (ps)
ZnTPP	1.4	1.4
TZn_3	1.0	1.0
TZn_3L	1.0	0.9
TZn_3D	0.93	0.9
HZn_6	< 0.15	0.4
HZn_3Fb_3[b]	< 0.15	~7[c]

[a] If not specified, the S_1 fluorescence was monitored at 620 nm. [b] Measured at 715 nm. [c] Relative amplitude: 0.42.

TABLE 3: Decay Parameters Obtained from the Analysis of the S_1 Fluorescence of the Arrays and of the Monomers[a]

compound	τ_1 (ns)	A_1	τ_2 (ps)	A_2	τ_3 (ps)	A_3
ZnTPP	1.8	1				
TZn_3	1.8	0.65	40	0.35		
TZn_3L	1.8	0.46	110	0.28	12	0.26
TZn_3D	1.8	0.68	220	0.19	16	0.13
HZn_6	1.7	0.18	85	0.16	20	0.66
HZn_6[b]	1.7	0.28	85	0.21	20	0.51
FbTPP[b]	12	1				
HFb_6[b]	11.9	0.37	450	0.21	32	0.42
HZn_3Fb_3	11.5	0.03	37	0.30	8.3	0.67
HZn_3Fb_3[c]	11.5	0.21	430	0.41	60	0.38

[a] If not specified the fluorescence was recorded at 620 nm. [b] Measured at 650 nm. [c] Measured at 715 nm.

The fluorescence of the triporphyrin arrays exhibits two main differences compared with ZnTPP: first, the S_2 lifetime and the corresponding S_1 fluorescence rise time are significantly shorter, and second, the S_1 fluorescence decay is no longer exponential (see Figure 5). The rise time of the S_1 fluorescence matches rather well the S_2 fluorescence lifetime. Although the 1.8 ns component observed with ZnTPP monomer is present in the S_1 decay of the triporphyrins, new faster components are present. For TZn_3, an additional 40 ps component is required to reproduce the S_1 fluorescence decay (see Figure 5). For TZn_3L and TZn_3D, the decay is more complex, and no reasonable fit can be realized with less than three exponential functions with lifetimes around 10−20 ps, 100−200 ps, and 1.8 ns.

The fluorescence dynamics of HZn_6 differs strongly from that of ZnTPP as well. Although no S_2 band could be seen in the steady-state fluorescence spectrum of this array, some fluorescence at 440 nm with an ultrafast decay could be measured by up-conversion. The lifetime of this emission, which is not due to Raman scattering, is significantly shorter than the response function of the setup. However, the rise of the S_1 fluorescence, measured at 620 nm, is markedly slower. The S_1 fluorescence decay of HZn_6 can also be reproduced with a three exponential function with time constants similar to those found with the triporphyrins (see Figure 6A). The same time constants are obtained at 650 nm, but the amplitudes are somewhat different, the relative amplitude of the faster component exhibiting a 20% decrease.

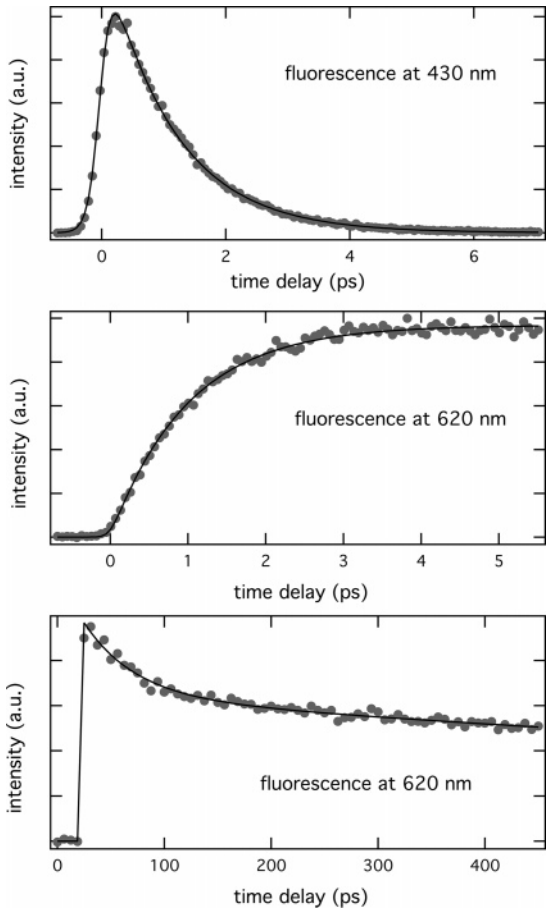

Figure 5. Time profile of the S_2 and S_1 fluorescence of TZn_3 measured upon 400 nm excitation.

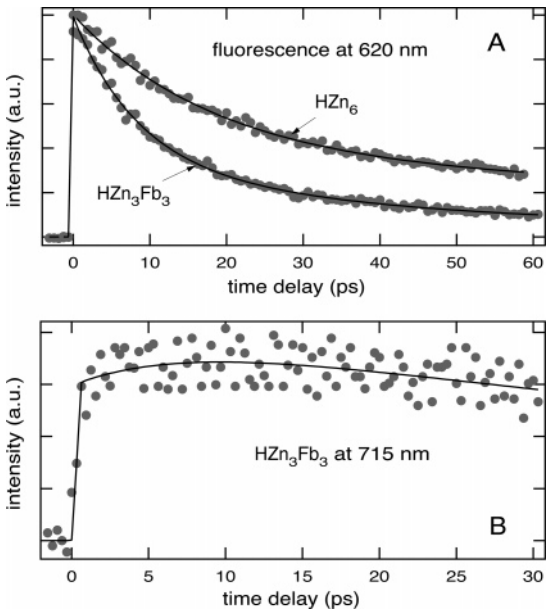

Figure 6. Time profiles of the fluorescence of (A) HZn_6 and HZn_3Fb_3 at 620 nm upon 400 nm excitation and (B) of HZn_3Fb_3 at 715 nm upon 430 nm excitation.

Upon 400 nm excitation, the S_1 fluorescence of FbTPP rises within the response time of the up-conversion setup. On the other hand, its decay at 715 nm is exponential with a 12 ns lifetime. At shorter wavelengths, relatively small ultrafast components that have been ascribed to vibrational relaxation can be observed.[53] Similarly to HZn_6, the fluorescence decay of HFb_6 at 715 nm cannot be reproduced by less than three exponentials with 30 and 450 ps time constants and with essentially the same time constant as that found with FbTPP.

TABLE 4: Parameters Obtained from the Analysis of the Dynamics of S_1 and S_2 Fluorescence Anisotropy Measured with ZnTPP and the ZnTPP Arrays (If Not Specified, the Limit of Error on τ_r is ± 10%)

	S_2 fluorescence		S_1 fluorescence	
compound	τ_r (ps)	$r_0 - r_f$	τ_r (ps)	$r_0 - r_f$
ZnTPP	0.25 ± 0.1	~ 0.4−0.1	150	0.1−0
TZn_3	0.25 ± 0.1	~ 0.4−0.05	80 ± 20	0.05−0
TZn_3L	0.25 ± 0.1	~ 0.4−0.1	2	0.1−0.04
TZn_3D	0.25 ± 0.1	~ 0.4−0.1	0.5	0.1−0.07
HZn_6			< 0.2	0.08−0.04
			16 ± 5	0.04−0.01

Similarly to HZn_6, the mixed hexamer HZn_3Fb_3 exhibits some fluorescence at 440 nm with an ultrafast decay upon excitation in the Soret band. In this case as well, the lifetime is significantly shorter than the response function of the experimental setup. At 620 nm, the emission originates from the ZnTPP chromophores only. The emission intensity rises within the instrument response time and exhibits a nonexponential decay that can also be reproduced by a triexponential function (see Figure 6A). Table 3 shows that the time constants associated with the ultrafast decay components are shorter than those found with HZn_6 and HFb_6 and that their relative amplitudes are larger. The lifetime of the slow component is unexpectedly very similar to that measured with the FbTPP monomer. However, some contamination of the emission at 620 nm by the fluorescence of the FbTPP units cannot be totally ruled out.

The fluorescence dynamics at 715 nm, where the emission is due to the FbTPP units, depends markedly on the excitation wavelength. This is due to the fact that the B-bands of the ZnTPP and FbTPP chromophores do not totally overlap, the B-band of ZnTPP being slightly red shifted relative to that of FbTPP. Upon excitation of HZn_3Fb_3 at 400 nm, about 80% of light absorption is in principle due to the FbTPP chromophores. In this case, the dynamics of the 715 nm fluorescence is very similar to that measured with HFb_6. Upon 430 nm excitation, about 68% of the absorption is due to the ZnTPP chromophores. In this case, the rise of the 715 nm fluorescence is biphasic as shown in Figure 6B. Indeed, in addition to a prompt rise, a slower rising component with a time constant of the order of 7 ps is observed. However, because of the weak pulse intensity at 430 and 860 nm, the signal-to-noise ratio of the data is quite poor and thus the uncertainty of the rise time is large. On the other hand, the fluorescence decay is very similar to that measured upon 400 nm excitation. The lifetime of the slow decay component is slightly smaller that those measured with HFb_6 and FbTPP.

Time-Resolved Fluorescence Anisotropy Measurements. The decay of the S_2 and S_1 fluorescence anisotropy of the ZnTPP arrays has been measured in order to obtain information on the dynamics of energy migration. For comparison, the same measurements have been performed with ZnTPP in toluene. The results are summarized in Table 4. The S_2 fluorescence anisotropy of ZnTPP has already been discussed in detail in the literature.[41,54,55] It decays with a time constant of the order of 250 fs from an initial value, r_0, of approximately 0.4 to a final value, r_f, of 0.1. The polarization anisotropy of the S_1 fluorescence upon 400 nm excitation starts from an initial value of about 0.1 and decays exponentially to zero with a time constant of 150 ps. A similar result has been found upon excitation in the Q-band. In this case, the anisotropy decay is due to the diffusional reorientation of ZnTPP in toluene.

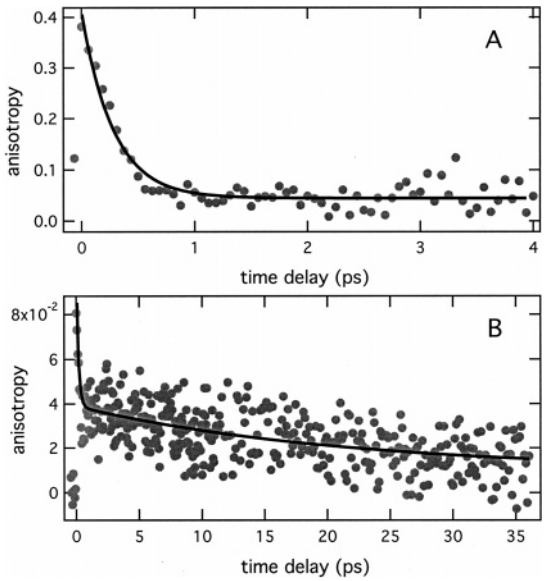

Figure 7. Time profile of (A) the S_2 fluorescence anisotropy of TZn_3 and of (B) the S_1 fluorescence anisotropy of HZn_6.

The dynamics of the S_2 fluorescence anisotropy of the triporphyrin arrays is very similar to that measured with ZnTPP. The only exception is TZn_3, for which the final anisotropy is smaller, around 0.05, as illustrated by Figure 7A.

The dynamics of S_1 anisotropy changes substantially from one array to another. Because of the rather small initial anisotropy, the data, especially those measured with TZn_3 and HZn_6, are very noisy, and therefore the error on the decay time is large. The S_1 fluorescence anisotropy decay of HZn_6 is shown in Figure 7B. The initial spike around time zero is reproducible and indicates that the anisotropy drops from about 0.08 to 0.04 in less than 200 fs. Then it decays to a value of 0.01 ± 0.01 with a time constant around 16 ps.

In the case of $TrZn_3$, the S_1 fluorescence anisotropy decays to zero with a time constant of the order of 80 ps. The S_1 anisotropy of the other two trimers, TZn_3L and TZn_3D, exhibits an ultrafast decay to 0.04 and 0.07, respectively. Then, it remains essentially constant up to a time delay of 50 ps. Anisotropy measurements on a larger time scale were not performed.

Discussion

Origin of the Differences between ZnTPP Monomer and ZnTPP Arrays. We will first discuss the results obtained with the ZnTPP arrays. When comparing with the ZnTPP monomer, the most important differences observed are the following: (1) the broadening of the Soret band, especially for the hexamer, (2) the shortening of the S_2 lifetime, and (3) the presence of new fast decay components of the S_1 fluorescence. Similar features have been observed with other porphyrin arrays. For example, in an investigation on the excited dynamics of a FbTPP hexamer, De Schryver and co-workers have observed a small broadening of the Soret band and a 20 ps component in the decay of the S_1-S_n transient absorption signal.[56] This component was attributed to the formation of an intramolecular interchromophoric excited state. More recently, Cho et al. have investigated the dynamics of ZnTPP dimer, trimer, and hexamer.[57] The trimer and hexamer differ from TZn_3 and HZn_6 by the absence of ethyne linker. A strong broadening of the Soret band and a decrease of the S_2 fluorescence lifetime with decreasing TS interchromophoric distance were observed. These two features have been attributed to excitonic interaction between the chromophores. Moreover, an additional fast decay component of the S_1 fluorescence was also measured upon Soret band excitation. The authors had no definitive explanation for this component and invoked energy transfer or conformational dynamics.

It is rather evident that most of the changes in the excited state dynamics found here by going from the ZnTPP monomer to the arrays must be related to the coupling between the chromophores and/or between the chromophores and the PA linkers. The dipole−dipole coupling energies, V_{12}, between two adjacent chromophores in the various arrays are listed in Table 5. The procedure used for these calculations is described in detail in the Supporting Information.

Table 5 shows that the coupling between the B transition dipoles of two adjacent chromophores in HZn_6 is very large and comparable to that found between the bacteriochlorophylls pigments B850 of the light-harvesting antenna of photosynthetic bacteria, where energy migration is discussed in terms of coherent excitons.[2] Therefore, the substantial broadening of the Soret band of the hexaporphyrins is most probably due to the presence of excitonic states of different energies. An estimation of the energy of the 12 excitonic states of HZn_6 is described in the Supporting Information and indicates that the lowest S_2 excitonic states are dark states. The presence of such dark states should strongly accelerate the nonradiative deactivation of the emissive state.[58,59] This could explain the very short S_2 fluorescence lifetime measured with HZn_6.

Table 5 also shows that the various differences observed between the triporphyrins and the monomer cannot be ascribed to the dipole−dipole coupling between the ZnTPP chromophores. Indeed, the excited state dynamics of the triporphyrins exhibits very similar features but the dipole−dipole coupling strength decreases strongly by going from TZn_3 to TZn_3L. If the electronic states of the chromophores are only very weakly perturbed by the proximity of another ZnTPP moiety, the substitution by the PA group might induce a stronger perturbation. This is confirmed by the FEA spectra shown in Figure 3. While the anisotropy measured with ZnTPP remains constant at 0.1 upon excitation over the whole B- and Q-bands, the anisotropy measured with TZn_3L and TZn_3D varies considerably through the B-band. This indicates that the B_x and B_y transition dipoles are no longer degenerate. Substitution along the *x*-axis should lead to a perturbation of B_x, while the perpendicular component, B_y, should remain essentially unaffected. The magnitude of this perturbation should be related to the size of the transition dipole. This could explain why the FEA spectra of TZn_3L and TZn_3D throughout the Q-band remain essentially constant. However, the shape of the FEA spectrum in the B-band region also implies that the $Q_{x,y}$ dipoles involved in the fluorescence at 600 nm are not strictly degenerate. Indeed, if they were degenerate, the anisotropy would be equal to 0.1 throughout the B-band, even though the B_x and B_y dipole moments are not degenerate.

The anisotropy value of 0.125 ± 0.01 measured in the FEA spectrum of TZn_3D in the Q-band region is a further indication that the Q_x and Q_y dipoles are no longer strictly degenerate. The same spectrum measured with TZn_3L is noisier but indicates an anisotropy larger than 0.1 as well.

In principle, the interaction between the PA linker and ZnTPP can occur via both the electrostatic and exchange mechanisms. However, the twist angle between the porphyrin and the linker should interrupt the π-conjugation to the detriment of the exchange interaction. As already mentioned above, the PA linker also acts as a chromophore, the energy of the lowest singlet

TABLE 5: Calculated Dipole−Dipole Coupling Energies and Calculated EET Time Constants for S_2 and S_1 Energy Transfer

	S_2 EET			S_1 EET		
array	V_{12} (cm^{-1})	τ_{EET}^{TS} (ps)	τ_{EET}^{TB} (ps)	V_{12} (cm^{-1})	τ_{EET}^{TS} (ps)	τ_{EET}^{TB} (ps)
TZn_3	52	0.8	42	4.4	912	332
TZn_3L	1.9	620	1.3×10^5	0.16	7×10^5	10^6
TZn_3D (PA_5-PA_3)	3.2	220	1.8×10^4	0.27	2.4×10^5	1.4×10^5
TZn_3D (PA_5-PA_1)	5.6	71	2500	0.47	8×10^4	2×10^4
TZn_3D (PA_3-PA_1)	14.3	11	315	1.2	1.2×10^4	2500
HZn_6	260	0.03	42	22	36	332
HZn_3Fb_3[a]	244	0.04	36	22	28	194[c]
HZn_3Fb_3[b]	244			22	3070	2.1×10^4

[a] EET from ZnTPP to FbTPP. [b] EET from FbTPP to ZnTPP. [c] From ref 40.

excited state decreasing with the number of PA units in para position. It has been shown that meta substitution disrupts the π-electron conjugation and leads to a localization of the excitation.[60,61] This property is at the origin of the efficiency of PA dendrimers as light-harvesting antennae.[62−65] Accordingly, the PA_3 linker should absorb around 375 nm, while the PA_5 linker should absorb just below 400 nm.[61] Moreover, their fluorescence spectrum should overlap quite well with the Soret band of the ZnTPP chromophores.[66] This should lead to a substantial electrostatic interaction between the transition dipole localized on the linker and the B_x dipole of the ZnTPP unit. The occurrence of this interaction is confirmed by the S_1 fluorescence excitation spectra of the ZnTPP arrays, which are identical to their absorption spectra even in the 300−400 nm region. This means that excitation of the PA linkers is followed by a very efficient EET to the porphyrin ends.

Consequently, the perturbation of the porphyrin by the linker is most probably at the origin of the differences observed in the absorption spectra of the triporphyrin arrays relative to the monomer and of the change of the relative intensity of the Q(0,0) and Q(0,1) emission bands. The shortening of the S_2 fluorescence lifetime measured with these arrays should also be related to this interaction. The magnitude of this interaction is not known, but it should not be large enough to lead to a delocalization of the excitation over the linker and the porphyrin. If it were the case, the absorption and emission spectra of the arrays in the B-band region should exhibit much larger differences relative to those of the monomer.

The presence of the short decay components of the S_1 fluorescence observed with all arrays is more difficult to explain. As the S_1 fluorescence quantum yield of the arrays is essentially the same as that of the monomer, these fast components are not due to additional nonradiative deactivation pathways of some fraction of the S_1 population but must rather be related to excited states that are populated by internal conversion from S_2. The main deactivation channel of these states should be the conversion to the S_1 state responsible for the 1.8 ns fluorescence decay component, that we will call the relaxed S_1 state, with time constants of the order of 20 and 110 ps, and the fluorescence to the ground state. Moreover, the fluorescence intensity from these states at the measured wavelength should be larger than that from the relaxed S_1 state. This implies that their fluorescence spectra differ from that of the relaxed S_1 state and/or that the corresponding oscillator strength is larger. In the case of HZn_6, the data listed in Table 3 indicate that the fluorescence spectrum from these "new" states is somewhat blue shifted relative to that from the relaxed S_1 state. The nature of the state is not clear. The shortest decay component could be related to vibrational cooling. It is however difficult to explain why this component is much larger with HZn_6 than with the triporphyrins and hardly visible with ZnTPP. In the case of HZn_6, this short component might also be connected to a localization of the energy after the decay of a S_2 excitonic state. However, this explanation cannot be applied to the triporphyrins. It is known that disorder can lift the degeneracy of the electronic states of aggregates composed of identical pigments. In this case energy hopping is directional and results in a dynamic red shift of the fluorescence, as the excitation is transferred from the pigments with the highest transition energy to those with the lowest transition energy. This process cannot be invoked here to explain the additional decay components of the S_1 fluorescence, because they are present on both sides of the emission band, although with different amplitudes. Conformational dynamics, as invoked by Cho et al.,[57] can also be a possibility. Moreover, the fact that there are two decay components does not obligatorily imply two conformations. It is indeed well-known that a distribution of decay times due to a distribution of conformations can often give rise to a decay that can be reproduced with a biexponential function.[67,68] In order to have a better insight into the origin of these additional components, fluorescence dynamics measurements at many different wavelengths between 430 and 700 nm should have been carried out. This was, however, not possible due to the limited amount of compound available. It should also be noted that the early fluorescence dynamics of ZnTPP upon Soret band excitation is itself rather complex, and its interpretation is still controversial.[51,69]

TABLE 6: Overlap Integrals between Normalized Donor Emission and Acceptor Absorption Spectra for S_2 and S_1 Energy Transfer

donor − acceptor	Θ (S_2)	Θ (S_1)
ZnTPP − ZnTPP	3.8×10^{-4}	4.8×10^{-5}
ZnTPP − FbTPP	3.4×10^{-4}	6.2×10^{-5}
FbTPP − ZnTPP		5.7×10^{-7}

Dynamics of the Fluorescence Anisotropy and of Energy Migration. The rather large dipole−dipole coupling energies calculated for some of the ZnTPP arrays should favor energy migration. The rate constant for TS EET through the Coulombic interaction, k_{EET}^{TS} can be calculated using a modified form of the Förster equation:[70]

$$k_{EET}^{TS} = 1.18 V_{12}^{\ 2} \int F_1(\nu) A_2(\nu)\, d\nu = 1.18 V_{12}^{\ 2} \Theta \qquad (3)$$

where k_{EET}^{TS} is expressed in ps^{-1}, the coupling energy is in cm^{-1}, and Θ is the overlap integral between the donor emission and acceptor absorption spectra with the area normalized to 1 on the cm^{-1} scale. The spectral overlap integrals for S_2 and S_1 EET between ZnTPP units are listed in Table 6. The time constants of TS EET, τ_{EET}^{TS}, calculated with eq 3 for the various arrays, are listed in Table 5.

This table predicts that TS EET should only be efficient in two ZnTPP arrays, namely HZn_6 and TZn_3. The interchro-

mophoric distance in the other arrays should prevent significant S_2 and S_1 energy migration. In a previous study on the S_1 EET in ZnTPP triporphyrins with increasing arm length (2.65 nm $\leq R_{TB} \leq$ 5.3 nm), it was shown that the TB exchange mechanism was operating as well.[40] For these arrays, the following distance dependence of the TB S_1 EET rate constant was estimated:

$$\ln k_{EET}^{TB}(S_1) \approx 25.8 - 1.5R_{TB} \quad (4)$$

where the TB distance R_{TB} is in nm. According to Dexter theory,[71] the rate constant for EET via the exchange mechanism is proportional to Θ. Therefore, if we assume that the molecular orbitals involved in the S_2 and S_1 EET are not too different, the rate constant of S_2 TB EET can be crudely estimated as

$$k_{EET}^{TB}(S_2) \approx k_{EET}^{TB}(S_1)\frac{\Theta(S_2)}{\Theta(S_1)} \quad (5)$$

The corresponding time constants, τ_{EET}^{TB}, for S_2 and S_1 EET are listed in Table 5. Here again, TB EET seems only to be a significant process in HZn_6 and TZn_3 in the S_1 state. The magnitude of the coupling energy between the $B_{x,y}$ dipoles in HZn_6 as well as the very small calculated τ_{EET}^{TS} indicate that S_2 energy migration in this array cannot be discussed in terms of incoherent transfer.[2] As mentioned above, the S_2 excitation must most probably be delocalized over several chromophores.

On the other hand, the data in Table 5 predict the occurrence of incoherent S_2 EET in $TrZn_3$ and S_1 EET in both $TrZn_3$ and HZn_6.

Energy migration in these arrays leads to a reorientation of the transition dipole moments and thus to a decrease of the fluorescence polarization anisotropy, *r*. The extent of anisotropy loss upon randomization of the excitation energy depends on the relative orientation of the ZnTPP chromophores and in particular on the twist angle φ, as discussed in detail in ref 40. For the triporphyrins, φ has been calculated to be 64°, and in this case, the residual anisotropy after EET should be smaller than 0.005.

The origin of the prompt drop of the S_1 fluorescence anisotropy decay of HZn_6 (see Figure 7B) is not clear. It might be related to a relocalization of the energy upon transition from the S_2 excitonic states to the S_1 state. Indeed, this prompt anisotropy change occurs within the rise of the S_1 fluorescence. Independently of this, the 16 ps component can be attributed to EET.

Assuming that EET from the initially excited porphyrin occurs only via TS interaction between adjacent chromophores, the S_1 fluorescence anisotropy should decay as follows (see Supporting Information):

$$r(t) = 0.025 + 0.075 \exp[-3k_{EET}^{TS}t] \quad (6)$$

An initial anisotropy value of 0.1 would most probably have been obtained experimentally if the S_1 state had been populated by direct excitation in the Q-bands. The final anisotropy measured experimentally is smaller but not very far from that calculated here. However, a distribution of twist angles φ within a single array and/or within the whole population is quite probable, and thus this difference should not be surprising. For the same reason, the calculation of this angle φ from the residual anisotropy is not meaningful. Despite these differences in the absolute anisotropy, the above relationship between the anisotropy decay time and the EET time constant holds. Therefore, the time constant for EET between the ZnTPP units in HZn_6 should be of the order of 48 $\pm$ 15 ps. This value compares rather well with that calculated from Förster theory and listed in Table 5. This indicates that the TB interaction is probably too weak compared with the TS interaction to contribute significantly to the anisotropy decay.

The same procedure can be used to analyze the decay of the polarization anisotropy measured with $TrZn_3$. Assuming a twist angle of 64°, the anisotropy should exhibit an exponential decay from 0.1 to almost zero with a time constant equal to $(3k_{EET})^{-1}$, with $k_{EET} = k_{EET}^{TS} + k_{EET}^{TB}$.[40] In this case, no assumption on the EET mechanism has to be made.

The S_2 fluorescence anisotropy of $TrZn_3$ decays from 0.4 to 0.05 with a time constant of the order of 250 fs. The randomization of the excited state population over the two degenerate states can only account for a decay to 0.1. Therefore, the residual anisotropy value of 0.05 could be interpreted as the occurrence of S_2 energy transfer. A look at Table 5 shows that eq 3 indeed predicts an 800 fs EET time constant. In this case, the time constant of the anisotropy decay due to EET should be of the order of 270 fs. If this was the case, the residual anisotropy should be essentially zero. Therefore, the S_2 EET should be somewhat slower than that calculated.

The decay of the S_1 fluorescence anisotropy of $TrZn_3$ is much slower. Because of the weakness of the initial anisotropy, only an approximate value of 80 ps can be estimated. The anisotropy decay of $TrZn_3$ upon Q-band excitation has already been investigated in detail using the crossed grating technique.[40] A decay time of 75 ps was obtained, in excellent agreement with that found here. From those measurements, an EET time constant of 225 ps was found. As discussed in ref 40, this value is substantially smaller than that calculated for TS EET (see Table 5), and therefore the difference can be attributed to the contribution of TB EET via the exchange mechanism.

The S_2 anisotropy decay measured with the other two triporphyrins is similar to that found with the ZnTPP monomer, indicating that S_2 EET is not operative. This is consistent with the relatively long calculated EET time constants listed in Table 5. The same table predicts that EET should not take place in $TrZn_3L$, independently of the mechanism. This agrees with the steady-state FEA spectrum of $TrZn_3L$, especially in the Q-band region, which exhibits a value close to 0.1 (see Figure 3). The steady-state anisotropy upon 400 nm excitation is smaller, because of the interaction with the spacer, as discussed above. The S_1 anisotropy dynamics upon 400 nm excitation exhibits a 2 ps decay from 0.1 to 0.04 and then remains constant. The presence of a residual anisotropy is a further confirmation that EET does not occur. The origin of the initial anisotropy decay is not clear. It must most probably be connected to the presence of the linker. In principle, the PA_5 linker could also be excited at 400 nm. Therefore, the 2 ps decay might be related to an EET from the linker to the porphyrin. The fluorescence excitation spectrum of TZn_3L shows that this process does indeed occur.

TZn_3D is an asymmetric array, and therefore there are in principle three distinct EET processes. Table 5 shows that EET should only be possible between the two porphyrins with PA_1 and PA_3 linkers. In this case, the anisotropy decay time should be twice as short as the EET time and should thus be of the order of 5.5 ps and 1.1 ns for S_2 and S_1 energy, respectively. This S_2 EET time is certainly too large compared to the S_2 lifetime to induce significant anisotropy decay, in agreement with the experiment. Moreover, the decrease of the anisotropy upon energy migration over two of the three chromophores is not as large as when the EET occurs between all three ZnTPP

moieties. Indeed, the calculated residual anisotropy after randomization of the excitation over two chromophores is still quite large and amounts to 0.042. This value as well as a rather slow EET explains the relative large intensity of the FEA spectrum in the Q-band region. The S_1 anisotropy upon 400 nm excitation exhibits an ultrafast decay from 0.1 to a value of 0.07, which remains constant over the time window of the experiment. In this case again, we have no definitive explanation for the ultrafast component. However, the rather large residual value agrees with an inefficient S_1 energy migration in this array.

Energy Transfer in HZn_3Fb_3. In principle, the EET dynamics in the mixed array HZn_3Fb_3 should be more easily accessible than in the ZnTPP arrays. This is however not really the case, because of the impossibility of selectively exciting the ZnTPP chromophores in the B-band region. Nevertheless, upon excitation at 430 nm the fluorescence time profiles at 620 nm and at 715 nm originating from the ZnTPP and the FbTPP units, respectively, give some evidence of the occurrence of EET between ZnTPP and FbTPP. First, the fluorescence decay at 620 nm is substantially faster than that measured with HZn_6 (see Figure 6A), and second, the early fluorescence dynamics at 715 nm exhibits, in addition to a prompt rise, a ~7 ps component that is not present in the FbTPP monomer (see Figure 6B). The prompt rise can be attributed to the direct excitation of the FbTPP chromophores at 430 nm. The longer rise time is close to the 8.3 ps lifetime found at 620 nm. The shortening of the decay time at 620 nm by going from HZn_6 to HZn_3Fb_3 can thus be attributed to an EET process with the following overall time constant:

$$\tau_{ov}^{-1} = \tau_3^{-1}(HZn_3Fb_3) - \tau_3^{-1}(HZn_6) \quad (7)$$

With the use of the τ_3 values listed in Table 3, an overall EET time constant of 14 ps is obtained. A look at the structure of HZn_3Fb_3 shows that there are two TS and three TB EET pathways. Consequently, the relationship between the overall EET time constant and the TS and TB EET time constants can be written as

$$\tau_{ov}^{-1} = 2(\tau_{EET}^{TS})^{-1} + 3(\tau_{EET}^{TB})^{-1} \quad (8)$$

This expression assumes that all three TB pathways are equivalent. This is certainly not the case, the TB coupling between chromophores in the para position being certainly larger than that between chromophores in the ortho position. Nevertheless, this expression will be used in order to have an estimate of the TS EET time constant. With the use of the value of $\tau_{EET}^{TB} = 194$ ps, as determined from a previous study,[40] the time constant of TS EET amounts to 36 ps. This value is in reasonable agreement with that calculated with the Förster expression (see Table 5).

However, it should be noted that the decay of the ZnTPP emission in HZn_3Fb_3 is not exponential, a 37 ps component with 30% relative amplitude and a very weak 11.5 ns component also being present. As mentioned above, the early biexponential decay (8.3 ps + 37 ps) could be interpreted as a distribution of decay times, related to a distribution of conformations.

The origin of the 11.5 ns component is most probably due to back EET from the FbTPP to the ZnTPP chromophores. Back EET can also explain why this long decay component is shorter than the 12 ns measured with the FbTPP monomer as well as the presence of a small (about 1%) contribution of ZnTPP emission to the steady-state fluorescence spectrum of HZn_3Fb_3 (see Figure 2B). In the case of a reversible EET, the fluorescence time profiles of the ZnTPP and FbTPP chromophores can be described by the set of equations used to analyze excimer or exciplex dynamics.[72] From these equations, one can obtain a decay time of 11.5 ns for the slow component of both ZnTPP and FbTPP emission by assuming an equilibrium constant for the EET between ZnTPP and FbTPP units of 120. This value is in excellent agreement with the ratio of the spectral overlap integrals of 110 calculated for ZnTPP → FbTPP and FbTPP → ZnTPP S_1 EET (see Table 6). The reversibility of the process is essentially due to the long excited state lifetime of the FbTPP chromophore. This is an important parameter for the choice of an efficient energy trap.

Table 5 shows that the $B_{x,y}$ dipole−dipole coupling between two adjacent chromophores in HZn_3Fb_3 is almost as large as that calculated for HZn_6. As the S_0-S_2 transition energies of ZbTPP and FbTPP are almost equal, this large coupling most probably results to a delocalization of the S_2 energy over several chromophores as well. Therefore, the relaxation from these excitonic states to the lower S_1 states might be accompanied by a relocalization of the energy on either a ZnTPP or a FbTPP unit. If there is no preferential relocalization, S_2 excitation would result in a randomization of the S_1 energy over the array.

Conclusions

The excited state properties of the covalently linked porphyrin arrays investigated here are very complex and differ substantially from those of the monomers. In the case of the hexaporphyrins, these changes should be mostly due to the electrostatic interaction between the porphyrin units. This interaction is large enough to lead to a delocalization of the S_2 energy. It is much smaller in the S_1 state, but sufficient to favor energy migration among ZnTPP units as well as from ZnTPP to FbTPP chromophores within a few tens of picoseconds. Moreover, this coupling also enables back energy transfer from the FbTPP to the ZnTPP moieties, a process that one generally wants to avoid when designing an efficient energy trap. In these hexaporphyrin arrays, the interactions occur mostly through space. Some of the features observed with the hexaporphyrins, such as a broadening of the B-band and a shortening of the S_2 lifetime, are also observed with all the triporphyrins, although to a lesser extent. In this case however, through-space interaction between the porphyrin units can clearly not be invoked. Most of the features observed with these arrays are ascribed to the perturbation of the chromophores by the phenylacetylene linker, which leads to a lifting of the degeneracy of the electronic states. Although it was not studied in detail, this interaction can be expected to increase with increasing length of the linker, that is, upon decreasing the energy gap between the lowest electronic state associated to the linker and the S_2 state of the porphyrin. Another consequence of this interaction is the very efficient energy transfer from the linker to the porphyrin unit. The very fast ensuing deactivation to the S_1 state ensures a total irreversibility of the process. The use of such "active" linkers may open interesting perspectives for the ultrafast transfer of energy over long distances.

Acknowledgment. This work was supported by the Fonds National Suisse de la Recherche Scientifique though project nr.200020-100014.

Supporting Information Available: Calculation of the dipole−dipole coupling energy and of the energy of the excitonic states of HZn_6 and derivation of eq 6. This material is available free of charge via the Internet at http://pubs.acs.org.

References and Notes

(1) Pullerits, T.; Sundström, V. *Acc. Chem. Res.* **1996**, *29*, 381.

(2) Sundström, V.; Pullerits, T.; van Grondelle, R. *J. Phys. Chem. B* **1999**, *103*, 2327.

(3) Damjanovic, A.; Ritz, T.; Schulten, K. *Int. J. Quantum Chem.* **2000**, *77*, 139.

(4) Hsu, C.-P.; Walla, P. J.; Head-Gordon, M.; Fleming, G. R. *J. Phys. Chem. B* **2001**, *105*, 11016.

(5) van Amerongen, H.; van Grondelle, R. *J. Phys. Chem. B* **2001**, *105*, 604.

(6) Herek, J. L.; Wohlleben, W.; Cogdell, R. J.; Zeidler, D.; Motzkus, M. *Nature* **2002**, *417*, 533.

(7) Cerullo, G.; Polli, D.; Lanzani, G.; De Silvestri, S.; Hashimoto, H.; Cogdell, R. J. *Science* **2002**, *298*, 2395.

(8) Salverda, J. M.; Vengris, M.; Krueger, B. P.; Scholes, G. D.; Czarnoleski, A. R.; Novoderezhkin, V.; Van Amerongen, H.; Van Grondelle, R. *Biophys. J.* **2003**, *84*, 450.

(9) Tabushi, I.; Sasaki, T. *Tetrahedron Lett.* **1982**, *23*, 1913.

(10) Overfield, R. E.; Scherz, A.; Kaufmann, K. J.; Wasielewski, M. R. *J. Am. Chem. Soc.* **1983**, *105*, 4256.

(11) Mialocq, J. C.; Giannotti, C.; Maillard, P.; Momenteau, M. *Chem. Phys. Lett.* **1984**, *112*, 87.

(12) Brookfield, R. L.; Ellul, H.; Harriman, A.; Porter, G. *J. Chem. Soc., Faraday Trans. 2* **1986**, *82*, 219.

(13) Nagata, T. *Bull. Chem. Soc. Jpn.* **1991**, *64*, 3005.

(14) Gust, D.; Moore, T. A.; Moore, A. L.; Gao, F.; Luttrull, D.; DeGraziano, J. M.; Ma, X. C.; Makings, L. R.; Lee, S.-J.; Trier, T. T.; Bittersmann, E.; Seely, G. R.; Woodward, S.; Bensasson, R. V.; Rougée, M.; De Schryver, F. C.; Van der Auweraer, M. *J. Am. Chem. Soc.* **1991**, *113*, 3638.

(15) Prathapan, S.; Johnson, T. E.; Lindsey, J. S. *J. Am. Chem. Soc.* **1993**, *115*, 7519.

(16) McCallien, D. W. J.; Sanders, J. K. M. *J. Am. Chem. Soc.* **1995**, *117*, 6611.

(17) Hsiao, J. S.; Krueger, B. P.; Wagner, R. W.; Johnson, T. E.; Delaney, J. K.; Mauzerall, D. C.; Fleming, G. R.; Lindsey, J. S.; Bocian, D. F.; Donohoe, R. J. *J. Am. Chem. Soc.* **1996**, *118*, 11181.

(18) Mongin, O.; Gossauer, A. *Tetrahedron* **1997**, *53*, 6835.

(19) Mongin, O.; Papamicaël, C.; Hoyler, N.; Gossauer, A. *J. Org. Chem.* **1998**, *63*, 5568.

(20) Biemans, H. A. M.; Rowan, A. E.; Verhoeven, A.; Vanoppen, P.; Latterini, L.; Foekema, J.; Schenning, A. P. H. J.; Meijer, E. W.; de Schryver, F. C.; Nolte, R. J. M. *J. Am. Chem. Soc.* **1998**, *120*, 11054.

(21) Piet, J. J.; Taylor, P. N.; Anderson, H. L.; Osuka, A.; Warman, J. M. *J. Am. Chem. Soc.* **2000**, *122*, 1749.

(22) Kuroda, Y.; Sugou, K.; Sasaki, K. *J. Am. Chem. Soc.* **2000**, *122*, 7833.

(23) Yeow, E. K. L.; Ghiggino, K. P.; Reek, J. N. H.; Crossley, M. J.; Bosman, A. W.; Schenning, A. P. H. J.; Meijer, E. W. *J. Phys. Chem. B* **2000**, *104*, 2596.

(24) Aratani, N.; Osuka, A.; Cho, H. S.; Kim, D. *J. Photochem. Photobiol., C* **2002**, *3*, 25.

(25) Kim, D.; Osuka, A. *J. Phys. Chem. A* **2003**, *107*, 8791.

(26) Yu, L.; Lindsey, J. S. *J. Org. Chem.* **2001**, *66*, 7402.

(27) Holten, D.; Bocian, D. F.; Lindsey, J. S. *Acc. Chem. Res.* **2002**, *35*, 57.

(28) Adams, D. M.; Brus, L.; Chidsey, C. E. D.; Creager, S.; Creutz, C.; Kagan, C. R.; Kamat, P. V.; Lieberman, M.; Lindsay, S.; Marcus, R. A.; Metzger, R. M.; Michel-Beyerle, M. E.; Miller, J. R.; Newton, M. D.; Rolison, D. R.; Sankey, O.; Schanze, K. S.; Yardley, J.; Zhu, X. *J. Phys. Chem. B* **2003**, *107*, 6668.

(29) Förster, T. *Ann. Phys.* **1948**, *2*, 55.

(30) Arnold, D. P.; Heath, G. A. *J. Am. Chem. Soc.* **1993**, *115*, 12197.

(31) Lin, V. S.-Y.; Therien, M. J. *Chem.—Eur. J.* **1995**, *1*, 645.

(32) Beljonne, D.; O'Keefe, G. E.; Hamer, P. J.; Friend, R. H.; Anderson, H. L.; Bredas, J. L. *J. Chem. Phys.* **1997**, *106*, 9439.

(33) Kumble, R.; Palese, S.; Lin, V. S. Y.; Therien, M. J.; Hochstrasser, R. M. *J. Am. Chem. Soc.* **1998**, *120*, 11489.

(34) Piet, J. J.; Taylor, P. N.; Wegewijs, B. R.; Anderson, H. L.; Osuka, A.; Warman, J. M. *J. Phys. Chem. B* **2001**, *105*, 97.

(35) Yeow, E. K. L.; Haines, D. J.; Ghiggino, K. P.; Paddon-Row: M. N. *J. Phys. Chem. A* **1999**, *103*, 6517.

(36) Yang, S. I.; Seth, J.; Balasubramanian, T.; Kim, D.; Lindsey, J. S.; Holten, D.; Bocian, D. F. *J. Am. Chem. Soc.* **1999**, *121*, 4008.

(37) Lammi, R. K.; Ambroise, A.; Balasubramanian, T.; Wagner, R. W.; Bocian, D. F.; Holten, D.; Lindsey, J. S. *J. Am. Chem. Soc.* **2000**, *122*, 7579.

(38) Cho, H. S.; Jeong, D. H.; Yoon, M.-C.; Kim, Y. H.; Kim, Y.-R.; Kim, D.; Jeoung, S. C.; Kim, S. K.; Aratani, N.; Shinmori, H.; Osuka, A. *J. Phys. Chem. A* **2001**, *2001*, 17.

(39) Tsai, H.-H.; Simpson, M. C. *Chem. Phys. Lett.* **2002**, *353*, 111.

(40) Brodard, P.; Matzinger, S.; Vauthey, E.; Mongin, O.; Papamicaël, C.; Gossauer, A. *J. Phys. Chem. A* **1999**, *103*, 5858.

(41) Gurzadyan, G. G.; Tran-Thi, T.-H.; Gustavsson, T. *J. Chem. Phys.* **1998**, *108*, 385.

(42) Muller, P.-A.; Högemann, C.; Allonas, X.; Jacques, P.; Vauthey, E. *Chem. Phys. Lett.* **2000**, *326*, 321.

(43) Morandeira, A.; Engeli, L.; Vauthey, E. *J. Phys. Chem. A* **2002**, *106*, 4833.

(44) Mongin, O.; Hoyler, N.; Gossauer, A. *Eur. J. Org. Chem.* **2000**, *2000*, 1193.

(45) Kalyanasundaram, K. *Photochemistry of Polypyridine and Porphyrin Complexes*; Academic Press: San Diego, CA, 1992.

(46) Quimby, D. J.; Longo, F. R. *J. Am. Chem. Soc.* **1975**, *97*, 5111.

(47) Ohno, O.; Kaizu, Y.; Kobayashi, H. *J. Chem. Phys.* **1985**, *82*, 1779.

(48) Sundström, V.; Gillbro, T.; Gadonas, R. A.; Piskarskas, A. *J. Chem. Phys.* **1988**, *89*, 2754.

(49) Gadonas, R.; Feller, K.-H.; Pugzlys, A.; Jonusauskas, G.; Oberlé, J.; Rullière, C. *J. Chem. Phys.* **1997**, *106*.

(50) Paillotin, G.; Swenberg, C. E.; Breton, J.; Geacintov, N. E. *Biophys. J.* **1979**, *25*, 513.

(51) Yu, H.-Z.; Baskin, J. S.; Zewail, A. H. *J. Phys. Chem.* **2002**, *106*, 9845.

(52) Gurzadyan, G. G.; Tran-Thi, T.-H.; Gustavsson, T. *Proc. SPIE* **2000**, *4060*, 96.

(53) Baskin, J. S.; Yu, H.-Z.; Zewail, A. H. *J. Phys. Chem.* **2002**, *106*, 9837.

(54) Wynne, K.; Hochstrasser, R. M. *Chem. Phys.* **1993**, *171*, 179.

(55) Razi-Naqvi, K.; Dale, R. E. *Chem. Phys. Lett.* **2002**, *357*, 147.

(56) Schweitzer, G.; DeBelder, G.; Latterini, L.; Karni, Y.; Rowan, A. E.; Nolte, R. J. M.; De Schryver, F. C. *Chem. Phys. Lett.* **1999**, *303*, 261.

(57) Cho, H. S.; Rhee, H.; Song, J. K.; Min, C.-K.; Takase, M.; Aratani, N.; Cho, S.; Osuka, A.; Joo, T.; Kim, D. *J. Am. Chem. Soc.* **2003**, *125*, 5849.

(58) van Amerongen, H.; Valkunas, L.; van Grondelle, R. *Photosynthetic Excitons*; World Scientific: Singapore, 2000.

(59) Spano, F. C.; Mukamel, S. *Phys. Rev. A* **1989**, *40*, 5783.

(60) Kopelman, R.; Shortreed, M.; Shi, Z.-Y.; Tan, W.; Xu, Z.; Moore, J. S.; Bar-Haim, A.; Klafter, J. *Phys. Rev. Lett.* **1997**, *78*, 1239.

(61) Tretiak, S.; Cherniak, V.; Mukamel, S. *J. Phys. Chem. B* **1998**, *102*, 3310.

(62) Devadoss, C.; Bharathi, P.; Moore, J. S. *J. Am. Chem. Soc.* **1996**, *118*, 9635.

(63) Bar-Haim, A.; Klafter, J.; Kopelman, R. *J. Am. Chem. Soc.* **1997**, *119*, 6197.

(64) Shortreed, M. R.; Swallen, S. F.; Shi, Z.-Y.; Tan, W.; Xu, Z.; Devadoss, C.; Moore, J. S.; Kopelman, R. *J. Phys. Chem. B* **1997**, *101*, 6318.

(65) Melinger, J. S.; Pan, Y.; Kleinman, V. D.; Peng, Z.; Davis, B. L.; McMorrow, D.; Lu, M. *J. Am. Chem. Soc.* **2002**, *124*, 12002.

(66) MacCallum, J. R.; Hoyle, C. E.; Guillet, J. E. *Macromolecules* **1980**, *13*, 1647.

(67) Siemiarczuk, A.; Wagner, B. D.; Ware, W. R. *J. Phys. Chem.* **1990**, *94*, 1661.

(68) Wlodarczyk, J.; Kierdaszuk, B. *Biophys. J.* **2003**, *85*, 589.

(69) Shibata, Y.; Chosrowjan, H.; Mataga, N.; Yoshida, N.; Osuka, A. In *Ultrafast Phenomena XII*; Elsaesser, T., Mukamel, S., Murnane, M. M., Scherer, N. F., Eds.; Springer: Berlin, 2000; p 689.

(70) Pullerits, T.; Hess, S.; Herek, J. L.; Sundström, V. *J. Phys. Chem. B* **1997**, *101*, 10560.

(71) Dexter, D. L. *J. Chem. Phys.* **1953**, *21*, 836.

(72) Hui, M.-H.; Ware, W. R. *J. Am. Chem. Soc.* **1976**, *98*, 4718.